Catalysis Communications 148 (2021) 106168

Contents lists available at ScienceDirect

Catalysis Communications

journal homepage: www.elsevier.com/locate/catcom

Short communication

Pt particles sintering on Pt/SiO_2 during water denitrification

A. Zaki, C. Lancelot, J.P. Dacquin, P. Granger*MethodologySupervisionWriting - original draftWriting - review & editing

Univ. Lille, CNRS, Centrale Lille, Univ. Artois, UMR 8181, UCCS - Unité de Catalyse et Chimie du Solide, F-59000 Lille, France

ARTICLE INFO

Keywords:
Pt sintering
Deactivation
Water denitrification
Silica-supported Pt
Mesoporous silica

ABSTRACT

Platinum particle growth in aqueous phase has been investigated at 20 °C in the course of nitrite (NO_2^-) reduction by H_2 reaction. A shift from a monomodal to a bimodal particle size distribution on used catalysts is accompanied with the disappearance of the smallest Pt particles in agreement with an Ostwald ripening mechanism. A two-step process involving consecutive dissolution and re- aggregation to form larger particles has been suggested according to a redox mechanism. Accordingly, the growth of large Pt particles at the expense of small ones induces a strengthening of the metallic character and a loss of Pt dispersion.

1. Introduction

Emerging catalytic applications in aqueous phase are often related to upgrading biomass-derived feedstock [1,2]. The complexity in such systems is usually associated to the solid/liquid /gas interfaces which makes difficult their optimization. In addition, the lack of relevant description of deactivation phenomena can limit further improvements on their durability. In case of metallic particles, supported on inorganic support materials, strong water adsorption can cause severe structural deteriorations and provoke particle sintering [3,4]. Ravanelle et al. [3] have shown a loss of stability of 1 wt% Pt/γ-Al_2O_3 and 1 wt% Ni/γ-Al_2O_3 catalysts during biomass reforming in aqueous phase at 200 °C assigned to a loss of acidic properties and specific surface area due to the transformation of γ-alumina to boehmite. All these changes led to Pd and Ni particle sintering. It is worthwhile to note that even for low-temperature applications, particle sintering is a serious obstacle.

Particle growth has been widely investigated in gas phase/solid catalytic reactions [5–7]. These processes were found highly activated at high temperatures. Douidah et al. [8] suggested an alternative sintering mechanism in aqueous phase. This differs from coalescence process or diffusion of metal atoms from the dissociation of small particles further aggregating through collisions with larger ones. Particle sintering on Cu/SiO_2 observed at 100 °C has been explained by a redox equilibrium in water where oxidic copper species undergo reduction on the largest Cu particles [9]. The lack of relevant observations at nanoscale is probably a critical point delaying the implementation of strategies to prevent and/or retard metal particle sintering. The development of environmental microscopic techniques led recently to appreciable information. Meijerink et al. [10] investigated particle dissolution and aggregation of gold nanoparticles in aqueous phase by *in situ* Transmission Electron Microscopy (TEM). They observed that a significant fraction of metallic particles was preserved keeping their original size. The time dependency of dissolution and particle growth sharply changes, the latter process being slow and likely rate-determining.

This study has been devoted to the stability of platinum particles on mesoporous silica materials in the course of water denitrification process. The reduction of nitrites by hydrogen was investigated on 1 wt% Pt/SiO_2 at 20 °C. TEM and XPS measurements led to convergent observations suggesting that a redox process could explain the changes observed on the particle size distribution partly related to deterioration of the mesoporous silica support under these operating conditions.

2. Experimental

2.1. Catalyst preparation and related physicochemical characterization

Hierarchical macroporous-mesoporous silica catalyst supports (called HS-X with X = polymer bead size) were prepared according to a dual-templating method as described elsewhere [11]. Polymer spheres as macro-template were impregnated by a pre-hydrolyzed solution containing the silica precursor and P123 block-copolymer for developing a mesoporous network. An intermediate composite nanospheres/P123-silica structure was obtained after soft hydrothermal treatment at 80 °C during 96 h. The final siliceous solids were obtained after calcination in air at 550 °C. Pt-HS-X catalysts were prepared by the wet

* Corresponding author.
E-mail address: pascal.granger@univ-lille.fr (P. Granger).

https://doi.org/10.1016/j.catcom.2020.106168
Received 23 June 2020; Received in revised form 6 September 2020; Accepted 8 September 2020
Available online 12 September 2020

impregnation method using hexachloroplatinic acid solution in order to obtain 1 wt% Pt (nominal loading). The impregnated precursors thus obtained were calcined in air at 400 °C and successively reduced at 300 °C or 450 °C in pure hydrogen overnight.

Transmission Electron Microscopy images were recorded on a JEOL JEM 2011 (LaB6) microscope and a FEI Tecnai G2 20 microscopes equipped with LaB_6 crystal and operating at a voltage of 200 kV. Textural properties were investigated based on nitrogen physisorption at −196 °C on an automated gas adsorption analyzer (Tristar 3020). The samples were degassed at 150 °C in vacuum for 3 h. Hydrogen chemisorption measurements were performed at room temperature by using a Micromeritics Autochem II 2920 apparatus. Prior to H_2 titration, the samples were preliminary reduced at 300 or 450 °C in pure hydrogen and then outgassed in flowing Ar at 400 °C for 1 h. Pt dispersion was calculated assuming $H/Pt_s = 1$. XPS measurements were carried out on an AXIS Ultra DLD Kratos spectrometer equipped with a monochromatized aluminium source for excitation (1486.6 eV). C1s core level at 284.8 eV was used as reference for binding energy (B.E.) correction.

2.2. Catalytic measurements

The experimental protocol was previously described [12]. Briefly, nitrites reduction experiments were performed in a semi-batch reactor continuously stirred at 20 °C. 0.08 g of catalyst, in powder form with average grain size of 250 μm, was suspended in 50 mL of nitrite solution obtained by dissolving 18.5 mg of KNO_2 in deionized water. The solution was subjected to a continuous feed of pure gaseous hydrogen. Aliquots of 1 mL were regularly sampled and analyzed by ionic chromatography using a Methrom (844 UV/VIS Compact IC) equipped with a Metrosep A Supp 16–150/4.0 column. The calculation of the Weisz-Prater criterion reported in Electronic Supporting Information (ESI) showed that internal mass transfer limitations could not be strictly ruled out in the estimates of initial specific rates reported in Table 1.

3. Results and discussion

3.1. Microscopic visualization of Pt particle growth

Fig. 1(a) shows TEM analysis on Pt-HS-200, pre-reduced at 300 °C, revealing practically a homogeneous Pt distribution in size in the whole volume of the supported catalyst particle. Related particle size distribution in Fig. 2(a) led to a mean Pt particle size of approximately 3.5 nm (see Table 1). Despite a dual-texturing, a monomodal distribution of metallic Pt particles is observed mostly distributed in the mesoporous network as evidenced by tomography analysis [13], in agreement with larger pore size. Similar monomodal Pt distributions were also found on Pt-HS-65 and Pt-HS-100 as reported in Fig. S1 (ESI) irrespective of the reduction temperature, *i.e.* 300 or 450 °C. Nevertheless, a noticeable particle sintering takes place leading to broader distribution and a shift to higher particles sizes when the pre-reduction is carried out at 450 °C (Fig. 2(b)).

Reaction medium induces drastic changes revealing in (Fig. 1(b)) strong heterogeneity of Pt particle sizes with different micro domains characterized by large particles and very small ones (zone 1), which seem unaffected by the operating conditions. Similar observations were recently reported on supported gold particles in aqueous phase from *in situ* TEM measurements [10]. Particle size distribution established over one hundred Pt particles (Fig. 2) reveals on used Pt-HS-200 catalyst a strong particle sintering of Pt particles which does not seem to be related to a collapse of the dual-texturing. Indeed, the microporous windows still appears distinctly in Fig. 1(b). The most relevant observation is probably related to a bimodal particle size distribution also characterized the Pt-HS-65 and Pt-HS-100 (see Fig. S1, ESI) appearing more distinctly when the catalysts are pre-reduced at 300 °C. A careful examination of Fig. 2(a) reveals that the small Pt particles significantly disappear inducing a shift to higher particle size of the whole distribution and the appearance of a large particle domains in the range 8–12 nm. Similar observations were described by Wu and Phillips [6] but in gas phase/solid catalytic reactions and at high temperatures.

Up to now, sintering mechanism has been described predominantly in solid-gas phase catalytic reactions at high temperatures. Coalescence and intra-particulate atomic transport involving volatile platinum-containing species are commonly described [14]. The coalescence process implies the migration of mobile species onto the support that collide and coalesce into larger particles. Regarding the intra-particulate atomic transport, small crystallites would disappear through volatilization for the benefit of larger ones thanks to collision process, because they are more energetically favored. Hence, the loss of metal atoms is slower than their capture on larger particles. However, in practice the shape of the particle size distribution should remain monomodal with a long tail toward smaller particle sizes, whereas coagulation process would induce a tail toward larger particles and with a fitting to a logarithmic distribution in case of coalescence [15]. The concepts developed for particle sintering mechanisms in gas and liquid phases present some analogies. They can be regarded through the Ostwald ripening mechanism involving the dissolution of small particles, the diffusion of the solubilized species and their collisions with large particles inducing their growth.

A crucial information lies in the stability of the silica support in the current operating conditions. Indeed, previous investigations showed a weak stability of silica in aqueous conditions [9,16]. Partial

Table 1
Comparison between surface and catalytic initial rate on Pt-HS-X.

Catalyst		SSA (m^2/g)	Pore vol. (cm^3/g)	$\varnothing_{meso}$ (nm)	$\varnothing_{macro}$ (nm)	Pt dispersion	Mean Pt^0 particle size (nm)[a]	Mean Pt^0 particle size (nm)[b]	Initial rate (mmol h^{-1} g^{-1})
Pt-HS-65	Calcined	620	1.39	4.3	59				
	Red. 300 °C					0.42	2.4	5.0	17.2
	Red. 450 °C					0.34	2.9	8.2	21.4
	After reaction	421	0.97	3.7	50	0.25	4.0	bimodal PSD	
Pt-HS-100	Calcined	660	1.87	4.0	74				
	Red. 300 °C					0.62	1.6	4.1	13.5
	Red. 450 °C					0.57	1.7	8.2	27.2
	After reaction	480	1.25	4.3	68	0.38	2.6	bimodal PSD	
Pt-HS-200	Calcined	430	0.89	3.9	185				
	Red. 300 °C					0.43	2.3	3.5	14.8
	Red. 450 °C					0.24	4.2	7.9	22.0
	After reaction	266	0.49	6.6	176	0.06	16.7	bimodal PSD	

[a] Calculated from H_2 chemisorption measurements assuming hemispherical particles.
[b] Calculated from TEM analysis over one hundred Pt particles.

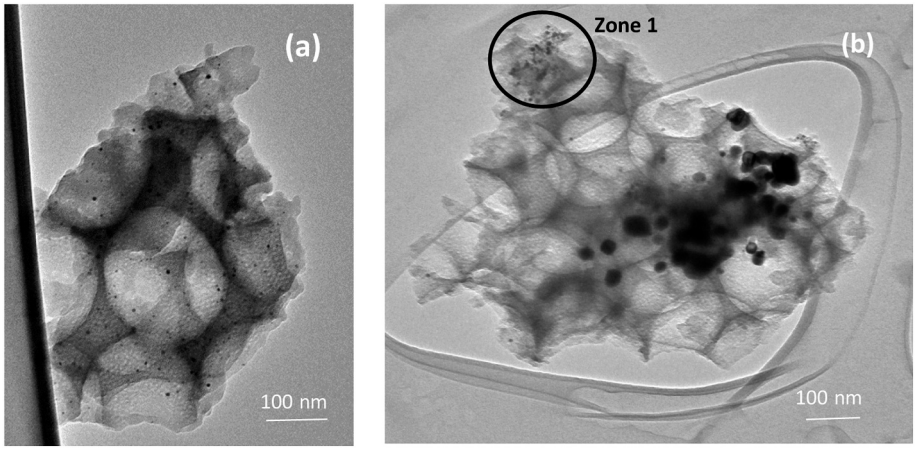

Fig. 1. TEM images recorded on Pt-HS-200 prereduced at 300 °C (a) and after reaction (b).

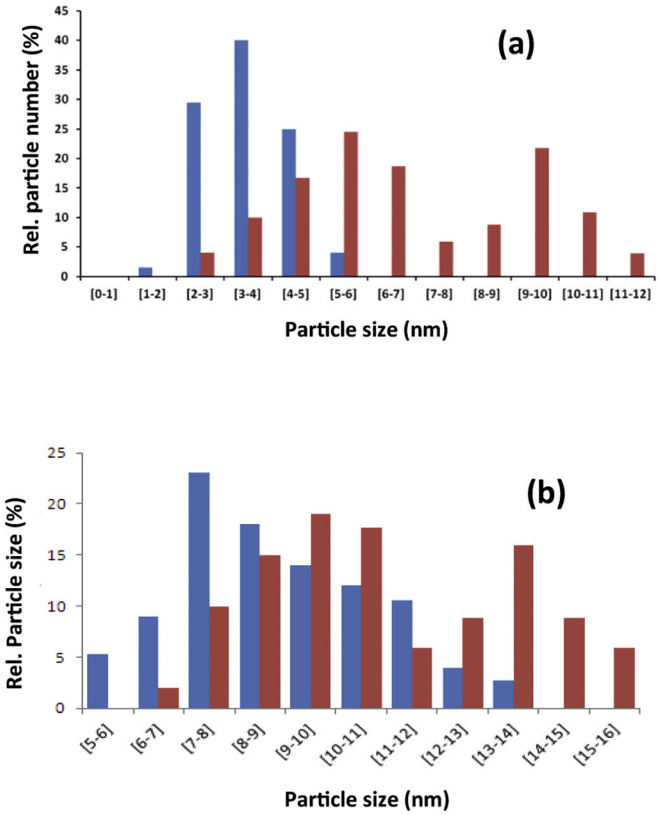

Fig. 2. Pt particle size distribution on Pt-HS-200 pre-reduced at 300 °C (a) and 450 °C (b) before reaction (blue) and after reaction (red). The statistical analysis was performed over one hundred Pt particles. (For interpretation of the references to colour in this figure legend, the reader is referred to the web version of this article.)

deterioration of the support could also weaken the Pt-silica interactions and then ease their migration onto the support in their immediate dissolution. As aforementioned, the dual porous structure is preserved but data in Table 1 clearly show an alteration of the textural properties associated to a partial loss of the pore volume and specific surface area, particularly on Pt-HS-200. These changes could contribute to the destabilization of the smallest Pt particles. Jointly, water can dissociate leading to -OH groups bonded to Pt particles. When metal–adsorbate interactions get stronger than the metal–support interactions then small metallic particles deteriorate, losing their metallic character more readily [5]. All these phenomena suggest that smaller Pt particles would be more subjected to dissolution in Pt-HS-X.

3.2. Do conversion profiles reflect deactivation in the course of water denitrification?

Meijerink et al. [10] argued that in the particle growth process, particle shrinkage would occur more readily, whereas the aggregation process would be slow and rate-determining. In other words, the disappearance of smaller particles would be much faster than their subsequent re-aggregation to larger particles. Accordingly, one can consider that these two processes could be temporarily decoupled with visible consequences on the conversion profiles of nitrites because this reaction is recognized as structure-sensitive and preferentially activated on zero valent Pt active sites [17].

Fig. 3 presents the nitrites conversion *vs.* time profiles recorded on catalyst samples pre-reduced at 300 and 450 °C. As summarized in Table 1, a pre-reduction in pure H_2 at higher temperature induced a loss of Pt dispersion and a growth of particle size estimated from H_2 chemisorption measurements. This evolution is consistent with TEM analysis revealing the same tendency on the mean Pt particle size shifting to larger values. Accordingly, a lower fraction of small metal particles would be subjected to deactivation when the catalysts are reduced at 450 °C. By comparing the conversion profiles recorded in the semi-batch reactor, one can observe that the catalytic performances of sample reduced at 450 °C outperform those obtained on samples pre-reduced at 300 °C. Higher initial specific rates on pre-reduced samples at 450 °C agree with the particle-size dependency of the rate earlier described with higher TOF values on larger particles [18]. Jointly, the preservation of more active metallic Pt sites could explain the evolution observed on the reaction rates [19].

A logarithmic function predicts conversion on samples reduced at 450 °C in agreement with a first order kinetics for the nitrite reduction by hydrogen reaction [20]. On the other hand, a polynomial function is more representative on samples pre-reduced at 300 °C, which could reflect the impact of the deactivation. It is also worthy to note that the two curves diverge at the early stage of the reaction, particularly on Pt-HS-65 and Pt-HS-100 pre-reduced at 300 °C with a stabilization of the conversion and a subsequent acceleration corresponding to higher instantaneous rates given by the slope of the straight line at the point of inflection. Such a behavior could be representative of different processes leading to a strengthening of the metallic character of sample initially pre-reduced at 300 °C through particle sintering. This behavior is less pronounced on Pt-HS-200 but a convergence toward comparable conversions is still observable.

All these observations seem to indicate that surface properties initially different according to the reduction temperature tend to equilibrate in the course of the reaction. Lower deviation observed on Pt-HS-

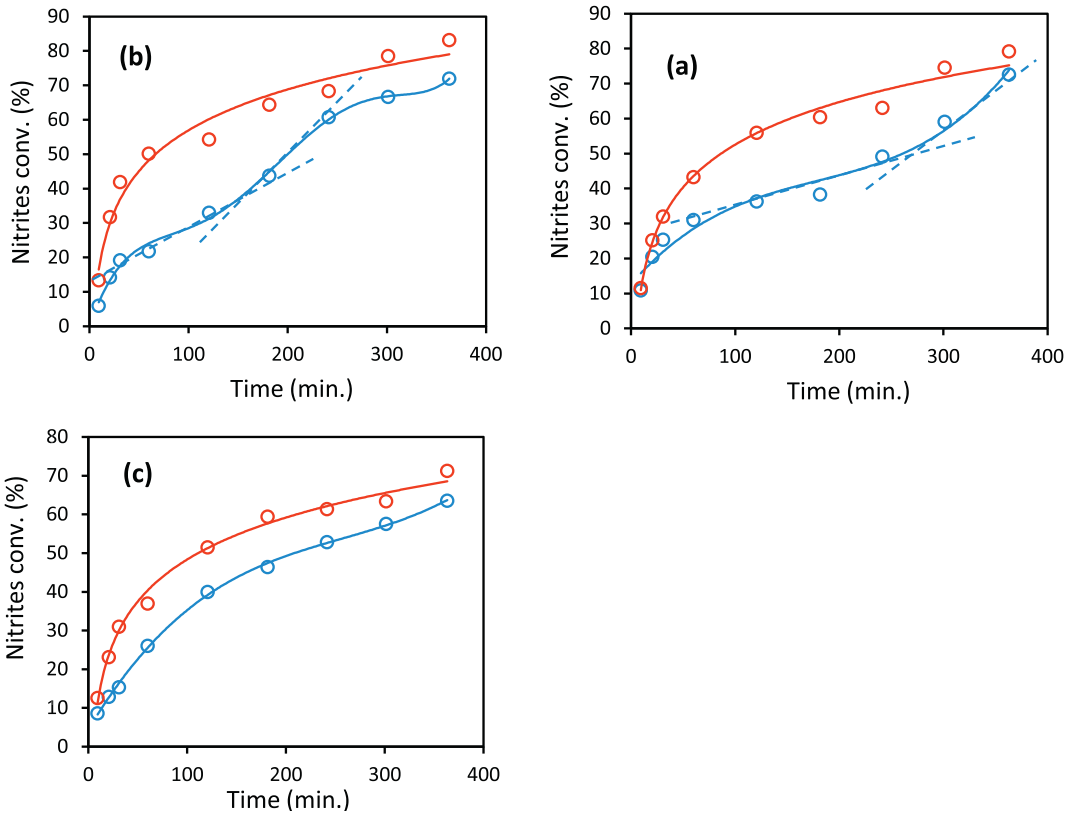

Fig. 3. Conversion *vs* time profiles in the course of nitrite reduction by hydrogen in semi-batch conditions on Pt-HS-65 (a), Pt-HS-100 (b) and Pt-HS-200 (c) catalysts pre-reduced at 300 °C (blue), and pre-reduced at 450 °C (red). Reaction conditions: 80 mg catalyst, $[NO_2^-]$ = 2.2 mmol/L, hydrogen flow rate = 200 mL/min. (For interpretation of the references to colour in this figure legend, the reader is referred to the web version of this article.)

200 could reflect a faster re-agglomeration process which seems in good agreement with the lowest Pt dispersion measured on the used catalyst. More open mesopores on used Pt-HS-200 could speed up the diffusion of soluble Pt^{n+} species, which seems consistent with previous conclusion emphasizing that particle sintering becomes slower when crystallite size tends to be similar to that of the pores [21].

3.3. Change in oxidation state of platinum: toward a strengthening of the metallic character on used catalysts

Ex situ XPS analysis complements previous observations showing that the nature of platinum species varies according to the pre-reduction temperature as well as after reaction. Particular attention was paid to the Pt 4f core level. Spectral data fitting (see Fig. S2, ESI) led to the isolation of three components on the Pt $4f_{7/2}$ with maxima at 71.1, 72.2 and 74.8 eV assigned to Pt^0, Pt^{2+} and Pt^{4+}, respectively. The presence of oxidic Pt species underlines surface re-oxidation of pre-reduced samples stored at ambient prior to XPS measurements. Their relative abundances change according to the reduction temperature, showing that larger Pt particles on pre-reduced samples at 450 °C are more resistant to re-oxidation in air. Nevertheless, a minor contribution of Pt^0 usually prevails (see Table 2).

Interestingly, Pt^0 species become predominant on Pt-HS-65 and Pt-HS-200 used samples, in agreement with the loss of Pt dispersion much more accentuated on Pt-HS-200. Jointly, there is no longer detection of Pt^{4+} species likely less stable than Pt^{2+} as previously pointed out, emphasizing that PtO_2 could diffuse at the surface or solubilize to further collide into larger particles [22]. This post-mortem characterization could suggest a particle sintering mechanism obeying to a redox process in aqueous phase [23,24]. A description can be given based on the redox mechanism described by Barbier et al. [23] for the preparation of bimetallic Pt—Au catalysts involving chemisorbed hydrogen atoms on Pt further reducing Au^{4+} to Au^0. As discussed in the Introduction, the growth of Cu particles in aqueous phase at 100 °C on Cu/SiO_2 has also been related to the reduction of solubilized Cu species on the largest Cu particles capable to chemisorbed hydrogen [9]. Ahluwalia et al. [24] complement these explanations combining in their model a non-ideal solid solution theory for depicting Pt dissolution and particle growth by the Ostwald ripening mechanism and coalescence process in the presence of hydrogen. Based on these arguments, Pt particles growth on Pt/SiO_2 during nitrite reduction by H_2 in aqueous phase would likely obey a redox process, as aforementioned with partial dissolution of smallest and unstable Pt particles, then soluble Pt^{n+} species with $n \geq 2$ would reduce on largest Pt^0 particles more stable and able to dissociate H_2. This could explain the progressive disappearance of small particles for the benefit of larger ones.

4. Conclusions

This study dealt with the origin of platinum particle growth in aqueous phase at 20 °C in the course of nitrite reduction by hydrogen reaction. Despite drastic changes in the operating conditions some analogies with particle sintering at high temperatures in gas/solid catalysis have been underlined. In gas phase, intra-particulate atomic transport involves the volatilization of small particles followed by collisions with large particles thermodynamically more stable. In aqueous phase, our observations match with the Ostwald ripening mechanism, involving a two-step dissolution of smaller particles and re-aggregation into larger particles corresponding to different time-scale. TEM, H_2-chimisorption and XPS analyses agree with the fact that instable Pt^{4+} species would be more prone to be converted into soluble species. These then would be subsequently reduced on large metallic Pt particles thanks to the presence of adsorbed atomic hydrogen. According to this redox process, the growth of large Pt particles at the expense of smaller ones would occur.

Table 2
XPS data recorded on Pt supported on silica exposed to different chemical environments.

Catalyst		Pt $4f_{7/2}$ (eV)	$(Pt/Si)_{surf}$	Relative abundance (%)		
				Pt^0 (71.1 eV)	Pt^{2+} (72.2 eV)	Pt^{4+} (74.8 eV)
Pt-HS-65	Calcined	71.3	0.23	12.1	63.1	24.8
	Red. 300 °C	71.5	0.46	11.8	42.4	45.8
	Red. 450 °C	71.5	0.36	33.7	48.5	17.8
	After reaction	71.5	0.38	56.8	43.2	–
Pt-HS-100	Calcined	71.1	0.23	10.6	66.5	22.9
	Red. 300 °C	71.3	0.42	18.1	46.4	35.5
	Red. 450 °C	71.5	0.46	21.2	56.6	22.1
	After reaction	71.1	0.38	36.9	63.1	–
Pt-HS-200	Calcined	72.2	0.16	25.4	43.9	30.7
	Red. 300 °C	72.2	0.12	36.4	42.9	20.7
	Red. 450 °C	71.2	0.10	49.9	26.1	21
	After reaction	71.3	0.26	56.9	43.1	–

Declaration of Competing Interest

The authors declare that they have no known competing financial interests or personal relationships that could have appeared to influence the work reported in this paper.

Acknowledgments

Chevreul Institute (FR 2638), Ministère de l'Enseignement Supérieur et de la Recherche and Région Hauts-de-France are acknowledged for supporting this work. The TEM facility in Lille (France) is supported by the Région Hauts-de-France and the European Regional Development Fund (ERDF).

Appendix A. Supplementary data

Supplementary data to this article can be found online at https://doi.org/10.1016/j.catcom.2020.106168.

References

[1] E.P. Maris, W.C. Ketchie, V. Oleshko, R.J. Davis, J. Phys, Chem. B 110 (2006) 7869–7876.
[2] F. Cai, D. Pan, J. Juweriah Ibrahim, J. Zhang, G. Xiao, Appl. Catal. A 564 (2018) 172–182.
[3] R.M. Ravenelle, J.R. Copeland, W.-G. Kim, J.C. Crittenden, C. Sievers, ACS Catal. 1 (5) (2011) 552–562.
[4] N. Dechamp, A. Gamez, A. Perrard, P. Gallezot, Catal. Today 24 (1995) 29–34.
[5] E. Ruckenstein, B. Pulvermacher, J. Catal. 29 (1973) 224–245.
[6] N.L. Wu, J.T. Phillips, J. Catal. 113 (1988) 129–143.
[7] P.C. Flynn, S.E. Wanke, J. Catal. 34 (1974) 390–399.
[8] A. Douidah, P. Marécot, J. Barbier Appl, Catal. A Gen. 225 (2002) 11–19.
[9] P. Granger, J.M. Dumas, C. Montassier, J. Barbier, J. Chim. Phys. 92 (1995) 1557–1575.
[10] M.J. Meijerink, K.P. de Jong, J. Zečevíc J. Phys. Chem. C 124 (3) (2020) 2202–2212.
[11] A. Zaki, Jing Xu, G. Stoclet, S. Casale, J.-P. Dacquin, P. Granger, Microporous Mesoporous Mater. 208 (2015) 140–151.
[12] P. Granger, S. Troncéa, J.P. Dacquin, M. Trentesaux, O. Gardoll, N. Nuns, V.I. Parvulescu, Appl. Catal. B 253 (2019) 391–400.
[13] J.P. Dacquin, P. Granger, A. Zaki, S. Casale, A. Mussi, J.F. Dhenin, C. Lancelot, Catal. Sci. Technol. 8 (2018) 4604–4608.
[14] S.E. Wanke, Catal. Rev. 1 (2) (1975) 93–135.
[15] C. Granqvist, R.A. Buhrman, J. Catal. 42 (1976) 477–479.
[16] A. Galarneau, M. Nader, F. Guenneau, F. Di Renzo, A. Gédéon, J. Phys, Chem. C 111 (2007) 8268–8277.
[17] J.K. Chinthaginjala, A. Villa, D.S. Su, B.L. Mojet, L. Lefferts, Catal. Today 183 (2012) 119–123.
[18] J.P. Dacquin, S. Troncéa, V.I. Parvulescu, P. Granger, Catal. Today (2020), https://doi.org/10.1016/j.cattod.2020.05.054 available online.
[19] M.-S. Kim, D.-W. Lee, S.H. Chung, J.T. Kim, I.-H. Cho, K.-Y. Lee, J. Mol, Catal. A 392 (2014) 308–314.
[20] A.M.E. Khalil, O. Eljamal, S. Jribi, N. Matsunaga, Chem. Eng. J. 287 (2016) 367–380.
[21] C.H. Bartholomew, Appl. Catal. A 212 (2001) 17–60.
[22] R.M.J. Fiedorow, S.E. Wanke, J. Catal. 43 (1976) 34–42.
[23] J. Barbier, P. Marecot, G. Del Angel, P. Bosh, J.P. Boitiaux, B. Didillon, J.M. Dominguez, I. Schifter, G. Espinoza, Appl. Catal. A 116 (1994) 179–186.
[24] R.K. Ahluwalia, S. Arisetty, J.-K. Peng, R. Subbaraman, X. Wang, N. Kariuki, D.J. Myers, R. Mukundan, R. Borup, O. Polevaya, J. Electrochem. Soc. 161 (3) (2014) F291–F304.